J Solid State Electrochem (2011) 15:391–397
DOI 10.1007/s10008-010-1103-z

ORIGINAL PAPER

The influence of Li sources on physical and electrochemical properties of $LiNi_{0.5}Mn_{1.5}O_4$ cathode materials for lithium-ion batteries

Tongyong Yang · Kening Sun · Zhengyu Lei · Naiqing Zhang · Ye Lang

Received: 16 March 2010 / Revised: 6 May 2010 / Accepted: 11 May 2010 / Published online: 23 May 2010

Abstract $LiNi_{0.5}Mn_{1.5}O_4$ cathode materials were successfully prepared by sol–gel method with two different Li sources. The effect of both lithium acetate and lithium hydroxide on physical and electrochemical performances of $LiNi_{0.5}Mn_{1.5}O_4$ was investigated by scanning electron microscopy, Fourier transform infrared, X-ray diffraction, and electrochemical method. The structure of both samples is confirmed as typical cubic spinel with *Fd3m* space group, whichever lithium salt is adopted. The grain size of $LiNi_{0.5}Mn_{1.5}O_4$ powder and its electrochemical behaviors are strongly affected by Li sources. For the samples prepared with lithium acetate, more spinel nucleation should form during the precalcination process, which was stimulated by the heat released from the combustion of extra organic acetate group. Therefore, the particle size of the obtained powder presents smaller average and wider distribution, which facilitates the initial discharge capacity and deteriorates the cycling performance. More seriously, there exists cation replacement of Li sites by transition metal elements, which causes channel block for Li ion transference and deteriorates the rate capability. The compound obtained with lithium hydroxide exhibits better electrochemical responses in terms of both cycling and rate properties due to higher crystallinity, moderate particle size, narrow size distribution and lower transition cation substitute content.

Keyword $LiNi_{0.5}Mn_{1.5}O_4$ · Oxide spinel cathode · High voltage · Lithium-ion battery · Li source

T. Yang · Z. Lei · Y. Lang
Department of Chemistry, Harbin Institute of Technology, Harbin 150001, People's Republic of China

K. Sun · N. Zhang (✉)
Academy of Fundamental and Interdisciplinary Sciences, Harbin Institute of Technology, Harbin, Heilongjiang 150001, People's Republic of China
e-mail: znqmww@163.com

K. Sun (✉)
State Key Laboratory of Urban Water Resource and Environment, Harbin Institute of Technology, Harbin, Heilongjiang 150090, People's Republic of China
e-mail: keningsun@yahoo.com.cn

Introduction

Lithium-ion battery is considered as an alternative to conventional power source for space devices, portable electronic devices, and electric vehicles (EV) owing to its high energy or power density as well as long cycle lifespan [1–4]. However, the performance and the utilization of batteries are limited by the property of cathode materials, so the investigation on the cathode material and the improvement of its performance attract considerable interest. $LiMn_2O_4$ spinel has been studied extensively as cathode material with economical and environmental advantages, such as low cost, low toxicity, and easy manufacture [5, 6]. However, the serious capacity decay upon cycling due to the Jahn–Teller effect of Mn^{3+} hinders its large-scale application in industry [7]. Substantive works focus on the replacement of Mn by substitute metals or surface coating for improving the performance. Among these approaches, $LiNi_{0.5}Mn_{1.5}O_4$ spinel is considered as an attractive candidate because the Ni^{2+} substitution not only overcomes the drawback of lattice distortion but also enlarges the working voltage window up to near 5 V [8]. For processions of the above merits, $LiNi_{0.5}Mn_{1.5}O_4$ is regarded as a promising 5 V class cathode material for high power EV applications.

It is well known that the physical and the electrochemical performances of cathode material are strongly dependent upon the synthesis method and the property of reagents [9]. $LiNi_{0.5}Mn_{1.5}O_4$ can be prepared with different methods, including molten salt method [10], sol–gel method [11, 12], solid-state method [13, 14], emulsion drying method [15], composite carbonate process [16], co-precipitation [17], and so forth. Among these methods, the sol–gel is recognized as an effective production technique in homogeneously mixing all reagents at atomic or molecular level, extremely allowing careful control of the stoichiometric amount and final particle size [18, 19]. Besides, the reagent selection is another factor for excellent performances. Recently, a series of $LiFePO_4$ cathodes were prepared with hydrothermal method. Their preferred crystal growth orientation and electrochemical performances could be significantly influenced by the adopted Li source [20]. In the case of $LiNi_{1-y}Co_yO_2$ specimens, the desired electrochemical behavior also could be obtained by choosing special Li source [21]. Accordingly, the selection of starting Li salt is of importance in the preparation of spinel with better behaviors. However, to the best of our knowledge, the effect of Li source on the performances of $LiNi_{0.5}Mn_{1.5}O_4$ spinel has not been reported yet.

In this paper, the spinel cathode material is prepared with sol–gel method using two different Li sources, and the effect of both starting salts on physical and electrochemical properties is discussed.

Experimental

Synthesis procedure

All chemical reagents used in this study were analytical reagent grade. $LiNi_{0.5}Mn_{1.5}O_4$ powders were prepared with sol–gel method. In brief, $LiOH{\cdot}H_2O$ or $LiOOCCH_3{\cdot}2H_2O$ (denoted as LiAC), $Ni(CH_3COO)_2{\cdot}4H_2O$, and $Mn(CH_3COO)_2{\cdot}4H_2O$ (cationic mole ratio of Li/Ni/Mn= 1:0.5:1.5) were dissolved in a continuously stirred aqueous solution of citric acid. After adjusting the pH of the solution to 7.0 by adding ammonium hydroxide, the solution was evaporated at 75 °C until a wet gel is obtained. Then, the gel was dried at 90 °C under vacuum atmosphere and pre-sintered at 450 °C for 5 h in air. Thereafter, the final powders were obtained by calcination at 850 °C for 18 h.

Physical characterization

The powder X-ray diffraction (XRD) was used to characterize the crystallographic structure of $LiNi_{0.5}Mn_{1.5}O_4$ powder on Rigaku D/max-2000 X-ray diffractometer with monochromated Cu K_α radiation (45 kV, 50 mA). Fourier transform infrared spectra (FTIR) of samples were performed on an Avatar 360 FTIR spectrophotometer (NICOLET) using KBr pellet technique. The particle morphology of powders was observed using a scanning electron microscope (SEM, HITACHI, S-4700). The differential scanning calorimetry (SETARAM, DSC141) was performed with a heating rate of 5 °C min^{-1} in air.

Electrochemical tests

The as-prepared $LiNi_{0.5}Mn_{1.5}O_4$, carbon black, and polyvinylidene fluoride were mixed with a weight ratio of 8:1:1 in *N*-methyl pyrrolidinone to prepare the positive electrode. The slurry was coated onto aluminum foil with doctor blade technique and dried at 120 °C for 12 h in vacuum, then dried again at 80 °C for more than 10 h in vacuum after being pressed. CR2025 button testing cells, using pure metallic lithium disk and $LiNi_{0.5}Mn_{1.5}O_4$ film as anode and cathode, porous polypropylene film as separator, respectively, were assembled in an argon-filled glove box. The electrolyte (1 M $LiPF_6$ in ethylene carbonate and dimethyl carbonate, 1:1 volume rate) was injected in testing batteries. A neware battery testing system (CT-3008W) was used for cycling and rate capability testing in the range from 3.0 to 4.95 V at specific rate (the calculated 1 C=148 mA g^{-1}) at room temperature.

Results and discussion

DSC analysis

Since the precursor strongly influences the particle nature of the produced material, Differential scanning calorimetry (DSC) measurements were performed for investigating the thermal decomposition behavior of both precursors composed of the acetate and the hydroxide, respectively. The experimental results are shown in Fig. 1, from which we can see similar curves are observed for both precursors, including an endothermic peak located at around 175 °C and two well-resolved exothermic peaks situated at the following high temperature range. The weak endothermic peak can be attributed to the removal of absorbed water [22], while the exothermic peak at the lower temperature position arises from the combustion of organic components in the precursor, and the other exothermic peak observed at the higher temperature location is caused by the formation of spinel [23]. It is worth noting that the exothermic peak at the lower temperature for the precursor prepared with LiAC is more intensive than that of precursor made from LiOH. This is due to the extra heat release from the acetate organic group in LiAC, since the preparation condition of both precursors is identical except for Li source. On the contrary, the other exothermic peak of the precursor comprising

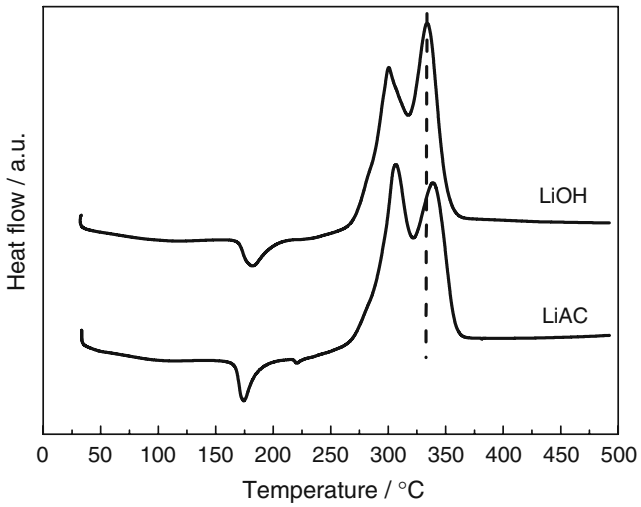

Fig. 1 DSC curves for the precursors prepared with LiAC and LiOH

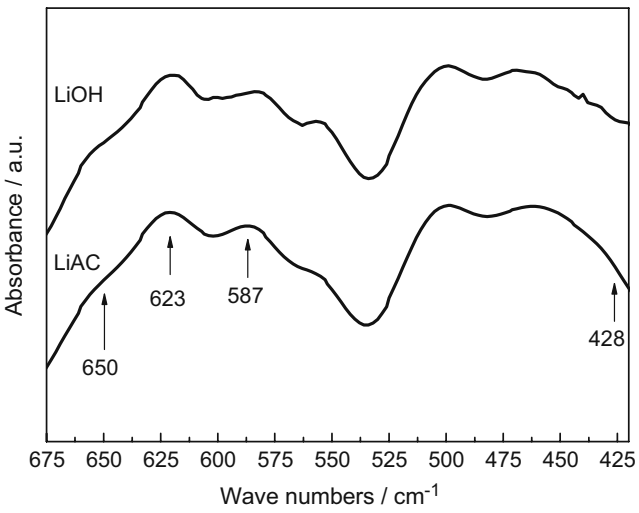

Fig. 3 FTIR spectra of the $LiNi_{0.5}Mn_{1.5}O_4$ spinels prepared with LiAC and LiOH

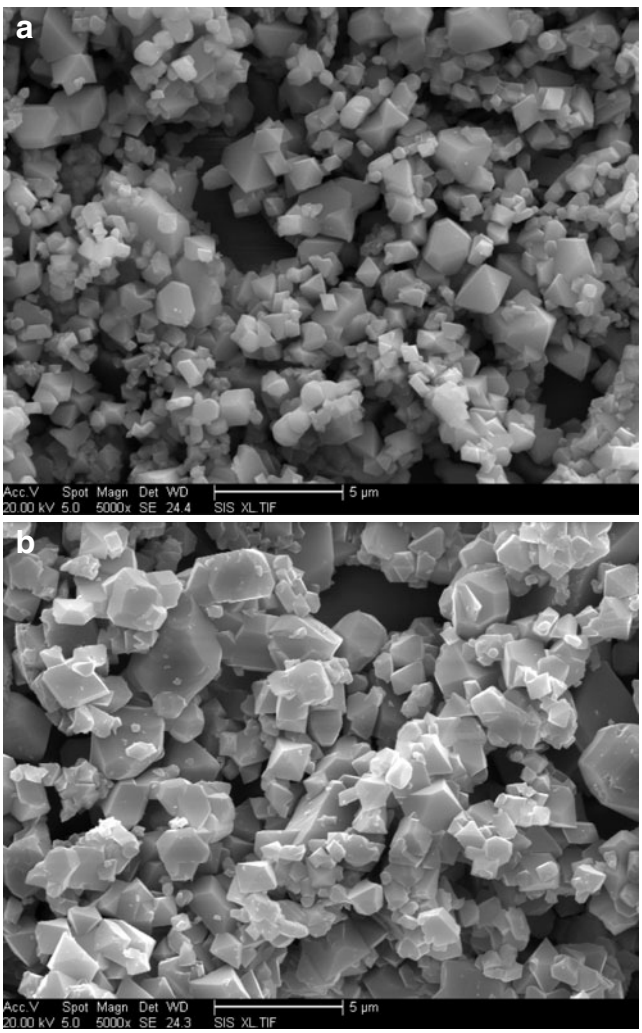

Fig. 2 SEM images of the $LiNi_{0.5}Mn_{1.5}O_4$ powders prepared with LiAC (**a**) and LiOH (**b**)

LiAC is weaker than that of the precursor based on LiOH and has a higher temperature shift. This indicates a lower crystal growth rate and is caused by the faster nucleation during the organic combustion process. It is reported that the crystal formation can be divided into nucleation and subsequent growth two processes, which occur simultaneously [24]. Accelerating the nucleation rate can restrain the growth rate since the provided stating sources are limited, and smaller particles can be obtained in the final powder [25]. In the case of LiAC precursor, greater heat released from the combustion of extra acetate organic component facilitates the nucleation, which further retards the crystal growth. Consequently, the sample prepared with LiAC should comprise considerable small particles, compared with the powder synthesized with LiOH.

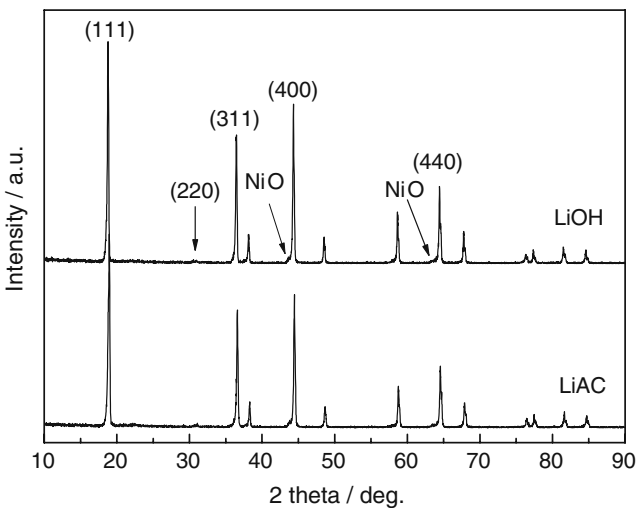

Fig. 4 XRD patterns of the $LiNi_{0.5}Mn_{1.5}O_4$ powders prepared with LiAC and LiOH

Table 1 Structure parameters of the $LiNi_{0.5}Mn_{1.5}O_4$ cathodes synthesized with LiAC and LiOH

Li sources	Lattice parameter (nm)	Unit cell volume (nm^3)	$I_{(311)}/I_{(400)}$
LiAC	0.8154	0.5421	0.92
LiOH	0.8170	0.5453	0.91

Morphology

SEM provides information about the surface morphology and homogeneity of the prepared $LiNi_{0.5}Mn_{1.5}O_4$ particle. Figure 2 shows the morphology of $LiNi_{0.5}Mn_{1.5}O_4$ prepared with different Li sources. The SEM observation indicates that the average particle size of the sample prepared with LiOH is about 2 μm (see Fig. 2b) and that of the other sample decreases to approximately 1 μm due to the appearance of considerably small particles with about 500 nm in size (see Fig. 2a). The result is consistent with the above DSC analysis, and the sample based on acetate has a relatively wider particle size distribution.

FTIR analysis

As well known, $LiNi_{0.5}Mn_{1.5}O_4$ spinel presents *Fd3m* and $P4_332$, two different space groups that are distinguished with each other by Ni ordering in the lattice [26]. FTIR is a local probe sensitive to the crystal symmetry and an effective approach to judge the ordering of cations [27]; here, the FTIR spectra of spinels obtained with different Li sources between 700 and 420 cm^{-1} are shown in Fig. 3. According to previous reports [28–30], more intensive band at 623 cm^{-1} compared with that at 587 cm^{-1}, and the absent or undefined bands at 650 and 428 cm^{-1} are special features for the space group of *Fd3m*. Accordingly, both cathode materials possess a disordered structure with a space group of *Fd3m*. The atom sites of this structure can be determined as that Li atoms occupy tetrahedral (8*a*) sites, Ni and Mn atoms are randomly located at octahedral (16*d*) sites, and O atoms are situated in octahedral (32*e*) sites [31, 32].

XRD analysis

XRD patterns of $LiNi_{0.5}Mn_{1.5}O_4$ powders prepared with different Li sources are shown in Fig. 4. All of the peaks in both X-ray diffraction patterns can be assigned to a cubic spinel structure. It is evidenced that the narrower full width at half maximum of peaks belongs to the sample prepared with LiOH, indicating a better crystallinity and larger particle size [33]. For both powders, very weak impurity peaks indexed to NiO are detected at the left shoulders of (4 0 0) and (4 4 0) diffraction peaks. This is an ordinary occurrence as the Ni content in spinel exceeds 0.2 [34] and originates from the oxygen release at high sintering temperature. Meanwhile, an accompanied reduction transition between Mn^{4+} and Mn^{3+} takes place for keeping electroneutrality. The appearance of weak (2 2 0) reflections demonstrates that some transition metal Mn ions are located in 8*a* sites with regard to the intense occupying propensity of Ni^{2+} ions in 16*d* sites, which can act as a deterrent for Li^+ diffusion [35]. Besides, Wang has pointed out that the increase in the intensity ratio of (3 1 1)/(4 0 0) reflects a more serious cation mixing [36]. For further understanding the crystal chemistry, the ratios and the lattice parameters are calculated and summarized in Table 1. As shown, the sample prepared with LiAC has larger ratio and smaller cell parameter than those of the sample based on hydroxide. This can be explained as that the radius of Li^+ at 8*a* site is larger than the transition metal element; thus, the replacement shrinks the cell volume, which further confirms the relatively serious transition cation substitution in the sample obtained with LiAC. The effect of Mn^{3+}, which has a larger radius than the oxidative Mn^{4+} ion, is neglected because of the same preparation conditions.

Electrochemical characterizations

The charge and discharge curves of $LiNi_{0.5}Mn_{1.5}O_4$ cathode materials prepared with both Li sources at 0.2 C rate are shown in Fig. 5. In order to better describe the electrochemical behavior, the fifth cycle is selected to avoid the interference from the electrode activation. It is clear that both electrochemical curves exhibit similar voltage plateaus at about 4.1 and 4.7 V, which are attributed to the Mn^{3+}/Mn^{4+}

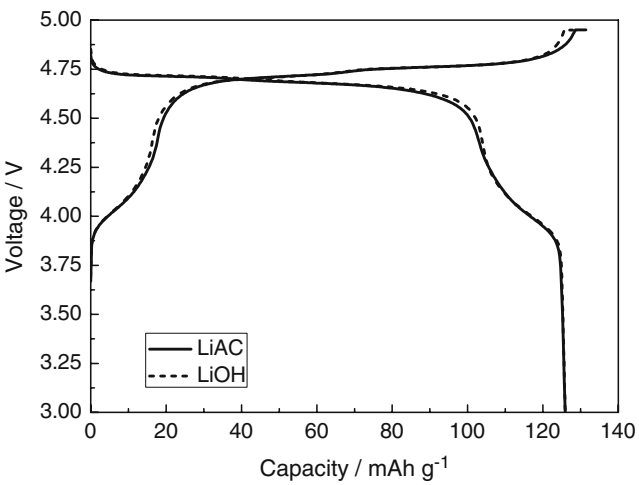

Fig. 5 Charge–discharge curves of the $LiNi_{0.5}Mn_{1.5}O_4$ cathodes prepared with LiAC and LiOH at 0.2 C

and Ni^{2+}/Ni^{4+} redox couples, respectively [37, 38]. Moreover, each charge curve consists of two close but distinct plateaus, which is a feature of the space group of *Fd3m* and consistent with the result of FTIR test [39]. Both cathodes exhibit an identical discharge capacity, which suggests that there is no difference in low rate discharge capability for the sample based on both Li sources. However, a less capacity is charged for the sample prepared with LiOH, indicating an advantageous efficiency.

The cycling performances of both as-prepared spinels measured at 0.2 C rate between 3.0 and 4.95 V versus Li are shown in Fig. 6. It is obvious that the compound prepared with LiOH has stable cycling behaviour, while the other presents an obvious capacity decrease upon cycling. The abrupt capacity decay can be explained by the small particle size, wide grain size distribution, as well as inferior crystallinity [10, 40, 41]. Small particles could supply larger surface area where the corrosion reaction occurs between the cathode surface and the electrolyte at the high operating voltage. Combined with the instable structure with poor crystallinity, the active material surface is more liable to be attacked by HF, which is one of the products of side reaction between the electrolyte and the trace H_2O and could reproduce during the corrosion process. The corrosion results in the dissolution of transition metal elements, the acceleration of electrolyte decomposition, the sequent deposition of inactive compounds on cathode surface, and finally, the deterioration of cyclability. However, for initial several cycles, the capacities of the electrode synthesized with LiAC surpass that of the other electrode with LiOH. Therefore, the small particle size benefits a higher beginning discharge capacity due to the fact that small particles are more reactive toward Li^+ ions [42]. The capacities after 40 cycles account for 89 and 96% of the maximum valve of cathodes fabricated with LiAC and LiOH, respectively.

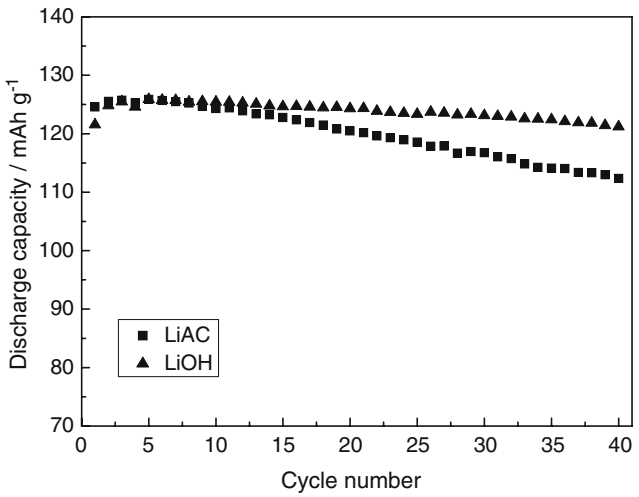

Fig. 6 Cycling performances of the $LiNi_{0.5}Mn_{1.5}O_4$ cathodes synthesized with LiAC and LiOH

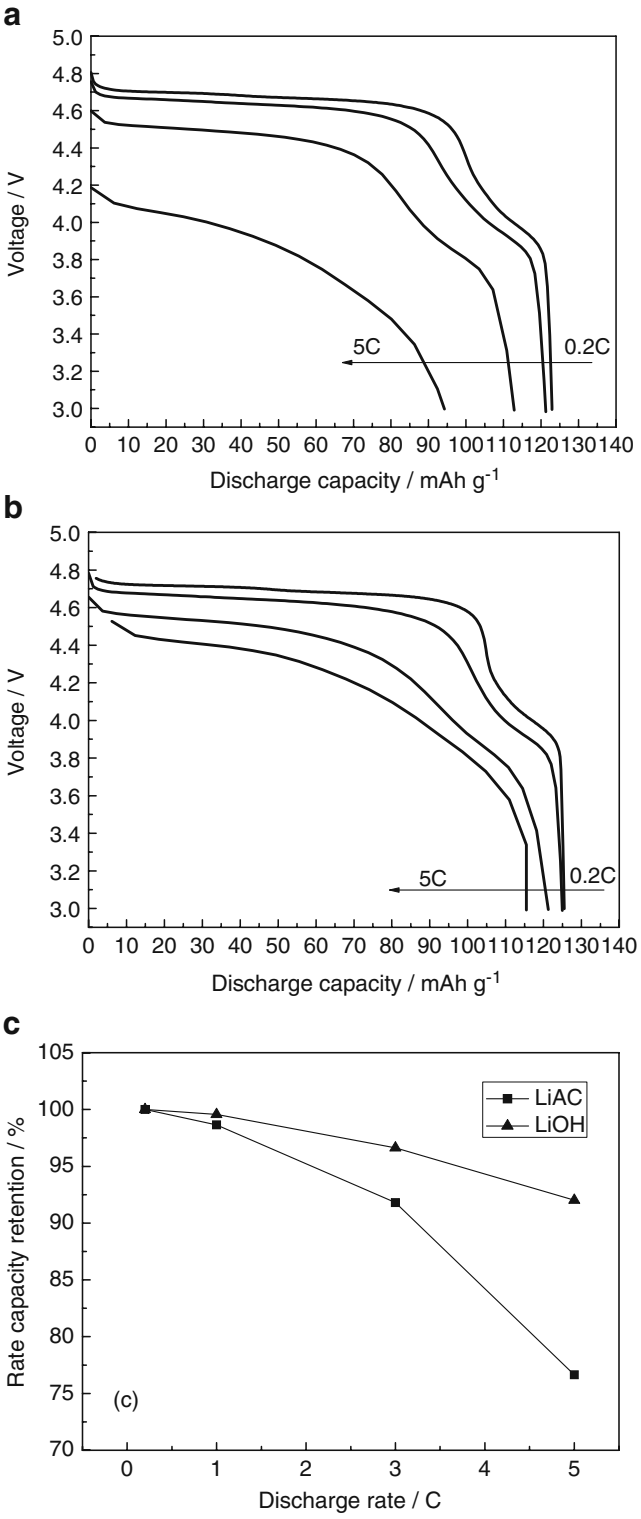

Fig. 7 Discharge profiles of the $LiNi_{0.5}Mn_{1.5}O_4$ cathodes synthesized with LiAC (**a**) and LiOH (**b**) at the rate of 0.2, 1, 3, and 5 C. Capacity retention comparison of the $LiNi_{0.5}Mn_{1.5}O_4$ cathodes synthesized with LiAC and LiOH at different rates (**c**)

The importance of high power applications requires battery possessions of high rate performance; therefore, galvanostatic discharge curves measured at different rates from 0.2 to 5 C between 3.0 and 4.95 V versus Li are plotted in Fig. 7. The cell is charged at 0.2 C rate before discharge test. With the discharge current increasing, cells generally exhibit a gradual decrease trend in discharge plateaus. The lowest plateau is observed for the electrode prepared with LiAC at the rate of 5 C, indicating an enormous polarization. The possible reason may be associated with the large replacing degree in Li sites by transition metal cations. In a spinel framework structure, transition metal ions at the tetrahedral sites normally impede lithium ion transportation; therefore, the Li ions are forced to travel tortuous paths, which leads to polarization at the condition of large current. The discharge capacities of the as-prepared $LiNi_{0.5}Mn_{1.5}O_4$ are 112.85 and 121.25 mAh g^{-1} at 3 C rate and 94.22 and 115.47 mAh g^{-1} at 5 C rate for the compound based on LiAC and LiOH, respectively. In order to reveal the rate capability of both cathodes, capacities have been assumed to be 100% capacity for the value measured at the rate of 0.2 C. The retentions of both cathodes as a function of discharge rate are presented in Fig. 7c. It is worth noting that the discharge capacity decays at the beginning low rates for both cathodes are relatively slow, while the capacity decays are rapid for the following high rates. However, over 90% of the initial capacity is maintained at 5 C for the electrode based on LiOH, while the counterpart is around 75%. The good rate performance can be attributed to the lower degree of cation mixing and the higher crystallinity, which is very important for maintaining the lithium ion diffusion pathway in the spinel structure [43].

Conclusions

In this study, spinel $LiNi_{0.5}Mn_{1.5}O_4$ cathode materials were successfully synthesized with sol–gel method. The effect of different Li sources, lithium acetate and lithium hydroxide, on physical and electrochemical properties of $LiNi_{0.5}Mn_{1.5}O_4$ cathode materials is discussed. The experimental results show that the precursor obtained with lithium acetate releases greater amount of heat during the precalcination process, which benefits the spinel nucleation. Consequently, the resultant powder possesses smaller average particle size and wider grain distribution, which results in high initial discharge capacity and severe capacity decay. The discharge behavior at 5 C rate is dramatically deteriorated due to more serious replacement in Li sites by transition metal elements. The sample prepared with lithium hydroxide exhibits stable cycling and outstanding rate performances on account of the high crystallinity and narrow particle size distribution. A high capacity retention accounting for 96% of the maximum is maintained after 40 cycles, and high discharge capacities of 121.25 and 115.47 mAh g^{-1} are obtained at the rate of 3 and 5 C, respectively. It is suggested that lithium hydroxide is an advisable Li source for the fabrication of $LiNi_{0.5}Mn_{1.5}O_4$ spinels in normal and high power applications compared with lithium acetate.

Acknowledgements This work was financially supported by the Funds for Creative Research Groups of China (no. 50821002).

References

1. Wu XL, Jiang LY, Cao FF, Guo YG, Wan LJ (2009) Adv Mater 21:2710–2714
2. Xie HM, Wang RS, Ying JR, Zhang LY, Jalbout AF, Yu HY, Yang GL, Pan XM, Su ZM (2006) Adv Mater 18:2609–2613
3. Tarascon JM, Armond M (2001) Nature 414:359–367
4. Kim DK, Muralidharan P, Lee HW, Ruffo R, Yang Y, Chan CK, Peng HL, Huggins RA, Cui Y (2008) Nano Lett 8:3948–3952
5. Taniguchi I (2005) Ind Eng Chem Res 44:6560–6565
6. Vidu R, Stroeve P (2004) Ind Eng Chem Res 43:3314–3324
7. Xiao LF, Zhao YQ, Yang YY, Cao YL, Ai XP, Yang HX (2008) Electrochim Acta 54:545–550
8. Ohzuku T, Takeda S, Iwanaga M (1999) J Power Sources 81–82:90–94
9. Kim JH, Myung ST, Sun YK (2004) Electrochim Acta 49:219–227
10. Sun YK, Hong KJ, Prakash J, Amine K (2002) Electrochem Commun 4:344–348
11. Alcántara R, Jaraba M, Lavela P, Tirado JL (2002) Electrochim Acta 47:1829–1835
12. Idemoto Y, Narai I, Koura N (2003) J Power Sources 119:125–129
13. Fang HS, Wang ZX, Li XH, Guo HJ, Peng WJ (2006) J Power Sources 153:174–176
14. Myung ST, Komaba S, Kumagai N, Yashiro H, Chung HT, Cho TH (2002) Electrochim Acta 47:2543–2549
15. Lee YS, Sun YK, Ota S, Miyashita T, Yoshio M (2002) Electrochem Commun 4:989–994
16. Fan YK, Wang JM, Ye XB, Zhang JQ (2007) Mater Chem Phys 103:19–23
17. Fu LJ, Liu H, Li C, Wu YP, Rahm E, Holze R, Wu HQ (2005) Prog Mater Sci 50:881–928
18. Liu ZQ, Wang WL, Liu XM, Wu MC, Li D, Zeng Z (2004) J Solid State Chem 177:1585–1591
19. Guo HJ, Li XH, Wang ZX, Peng WJ, Cao X, Li HF (2009) J Power Sources 189:95–100
20. Kanamura K, Koizumi S, Dokko K (2008) J Mater Sci 43:2138–2142
21. Song MY, Song J, Bang EY, Mumm DR (2009) Ceram Int 35:1625–1631
22. Liu JJ, Qiu WH, Yu LY, Zhao HL, Li T (2008) J Alloys Compd 449:326–330
23. Hon YM, Lin SP, Fung KZ, Hon MH (2002) J Eur Ceram Soc 22:653–660
24. Bhuiyan MIH, Mavinic DS, Beckie RD (2008) J Cryst Growth 310:1187–1194
25. Lin RY, Zhang JY, Zhang PX (2002) J Cryst Growth 245:309–320
26. Kim JH, Myung ST, Yoon CS, Kang SG, Sun YK (2004) Chem Mater 16:906–914

27. Alcantara R, Jaraba M, Lavela P, Trado JL, Zhecheva E, Stoyanova R (2004) Chem Mater 16:1573–1579
28. Kunduraci M, Al-Sharab JF, Amatucci GG (2006) Chem Mater 18:3585–3592
29. Liu J, Manthiram A (2009) J Electrochem Soc 156:A66–A72
30. Fang HS, Li LP, Li GS (2007) J Power Sources 167:223–227
31. Oh SW, Park SH, Kim JH, Bae YC, Sun YK (2006) J Power Sources 157:464–470
32. Nieto S, Majumder SB, Katiyar RS (2004) J Power Sources 136:88–98
33. Aklalouch M, Rojas RM, Rojo JM, Saadoune I, Amarilla JM (2009) Electrochim Acta 54:7542–7550
34. Zhong QM, Bonakdarpour A, Zhang MJ, Gao Y, Dahn JR (1997) J Electrochem Soc 144:205–213
35. Arrebola JC, Caballero A, Cruz M, Hernán L, Morales J, Castellón ER (2006) Adv Funct Mater 16:1904–1912
36. Wang HL, Xia H, Lai MO, Lu L (2009) Electrochem Commun 11:1539–1542
37. Park SB, Eom WS, Cho WI, Jang H (2006) J Power Sources 159:679–684
38. Markovsky B, Talyossef Y, Salitra G, Aurbach D, Kim HJ, Choi S (2004) Electrochem Commun 6:821–826
39. Takahashi K, Saitoh M, Sano M, Fujita M, Kifune K (2004) J Electrochem Soc 151:A173–A177
40. Hwang BJ, Wu YW, Venkateswarlu M, Cheng MY, Santhanam R (2009) J Power Sources 193:828–833
41. Raja MW, Mahanty S, Basu RN (2009) Solid State Ionics 180:1261–1266
42. Arrebola JC, Caballero A, Hernán L, Morales J (2005) Electrochem Solid-State Lett 8:A641–A645
43. Takahashi Y, Sasaoka H, Kuzuo R, Kijima N, Akimoto J (2006) Electrochem Solid-State Lett 9:A203–A206